

Structural analysis reveals formation and role of RNA G-quadruplex structures in human mature microRNAs

Received 00th January 20xx,
Accepted 00th January 20xx

Ka Lung Chan^{a,†}, Boya Peng^{b,†}, Mubarak I. Umar^a, Chun Yin Chan^a, Aleksandr B. Sahakyan^c, Minh T.N. Le^{b, #} and Chun Kit Kwok^{a, #}

DOI: 10.1039/x0xx00000x

www.rsc.org/chemcomm

Here we identify hundreds of RNA G-quadruplex (rG4) candidates in microRNAs (miRNAs), characterize the miRNA structure and miRNA-mRNA interactions on several mammalian-conserved miRNAs, and reveal formation of rG4s in miRNAs. Notably, we study the effect of these rG4s in cells and uncover the role of rG4s in miRNA-mediated post-transcriptional regulation.

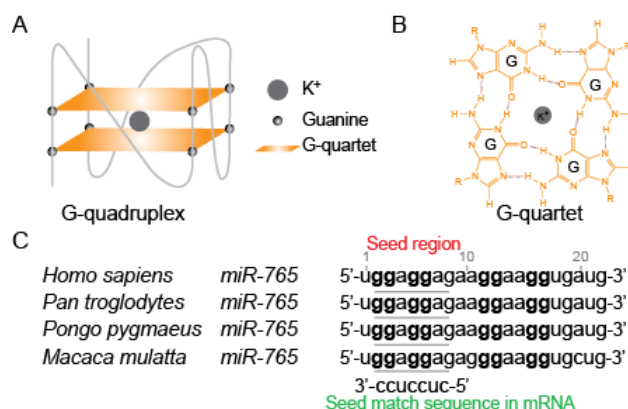
Guanine (G)-rich sequences in RNA can fold into non-canonical structural motifs called RNA G-quadruplexes (rG4s) (Figure 1A). These rG4 structures are composed of two or more G-quartets that are stabilized by potassium ion (K^+) (Figure 1B), and are linked by loop sequences of varying lengths (L)^{1, 2}. rG4s have been demonstrated to play important roles in fundamental biological processes such as gene regulation and RNA metabolism, and are associated with diseases including cancers and neurological disorders²⁻⁴. Transcriptome-wide sequencing results suggested that *in vitro* rG4s formation is prevalent in the human transcriptome^{5, 6}, and cell imaging experiments using G-quadruplex-specific antibody (BG4) have detected rG4s in fixed human cells⁷. Although transcriptome-wide structure probing in cells suggests rG4 are globally unfolded at steady-state⁶, recent real-time live cell imaging data using rG4-specific fluorescent turn-on chemical probe (QUMA-1) suggest that rG4s are highly dynamic and tightly regulated by cellular factors such as DHX36 RNA helicase in cells⁸.

Numerous studies have demonstrated the formation and function of rG4s in messenger RNA (mRNA)⁹, such as 5' untranslated region (UTR) rG4s in *NRAS* and *BCL2*, as well as 3'UTR rG4s in *PIM1* and *APP* that inhibit translation¹⁰⁻¹³. Recently, rG4s in non-coding RNAs have been identified and characterized³, for example *TERC*, *TERRA*, and *GSEC* long non-coding RNA, as well as several examples in primary microRNAs (pri-miRNAs) and precursor microRNAs (pre-miRNAs)¹⁴⁻¹⁹. These findings have illustrated the important roles of rG4s in both the coding and the non-coding transcriptome.

Mature microRNAs (miRNAs or miRs) belong to a class of small non-coding RNAs that are ~22 nucleotides in length, which have crucial roles in post-transcriptional regulation²⁰. Recent studies have suggested the *in vitro* formation of rG4 in

human miRNAs^{21, 22}, however, the current structural information of rG4 formation in miRNAs is very limited and of low resolution, and the cellular roles of the rG4s in miRNAs remain elusive. Herein, we perform bioinformatics, biophysical and biochemical approaches to identify and characterize rG4s in miRNAs, reporting rG4 structures in miRNAs, as well as miRNA-mRNA interactions at single nucleotide resolution for the first time. We further examine the importance of rG4s in miRNAs using reporter gene assays and reveal the cellular role of rG4s in miRNA-mediated post-transcriptional regulation.

Figure 1. RNA G-quadruplex structure in a mature microRNA. A) Schematic representation of an RNA G-quadruplex structure with parallel topology and two G-quartets. B) Chemical structure of a G-quartet, with potassium ion (K^+) at the center. C) Sequences of mature miR-765. The human miR-765 sequence is conserved in several mammalian species. The Gs involved in the putative G-quadruplex are in bold. The microRNA seed region (nucleotides 2-8) that interacts with the seed match sequence in mRNA (7 nucleotides) is underlined.



To examine the prevalence and potential rG4 formation in miRNAs, we first surveyed the miRBase²³ version 22 to identify miRNAs that contain putative rG4s (Table S1, ESI†). This identified up to 478 rG4-positive human miRNAs while using artificial neural network-based G4-detection algorithm G4NN, developed specifically for RNA sequences²⁴. To increase the stringency of the rG4 search in miRNAs, we considered only the 166 sequences that were positive based on both the above model and the Quadparser-based²⁵ (G_2N_{1-12})₃ G_{2+} sequence motif (denoted as G2L12 motif). We next selected 4 miRNAs (miR-149, miR-197, miR-432 and miR-765) to perform further experiments in this study. The selection was done based on their biological relevance, belonging to the high-confidence rG4 candidates, their general conservation pattern across mammalian species (Table S2, ESI†), and representation of various G4NN probabilities (Table S1, ESI†) in the rG4-positive

^a Department of Chemistry, City University of Hong Kong, Kowloon Tong, Hong Kong SAR, China. Email: C.K.K. (ckkwok42@cityu.edu.hk)

^b Department of Biomedical Sciences, City University of Hong Kong, Kowloon Tong, Hong Kong SAR, China. Email: M.T.N.L. (mle.bms@cityu.edu.hk)

^c MRC WIMM Centre for Computational Biology, Weatherall Institute of Molecular Medicine, Radcliffe Department of Medicine, University of Oxford, Oxford, OX3 9DS, United Kingdom

[†] These authors contributed equally to this work.

[#] These authors are corresponding authors.

Electronic Supplementary Information (ESI) available: See DOI: 10.1039/x0xx00000x

0.5 to 1.0 range²⁴ (0.997, 0.665, 0.549 and 0.717 for miR-149, miR-197, miR-432 and miR-765 sequences correspondingly). Notably, dysregulation of miR-765 has been shown to be associated with various cancers²⁶⁻²⁸, including human liver cancer, prostate cancer, and bone cancer.

To assess whether the putative rG4 sequences in miR-765 and other 3 miRNA candidates fold into rG4 structural conformation in physiologically relevant conditions, and to do so in a simple-to-setup *in vitro* system, we have adapted and refined the RNA ILP assay in multiple ways. In particular, we used i) physiologically relevant temperature at 37°C (versus room temperature²⁹); ii) physiologically relevant ionic concentration at 150 mM K⁺ (versus lower K⁺²⁹); iii) safe and commonly available FAM fluorescent label (versus radioactive ³²P or expensive, less popular fluorophores^{29, 30}).

In-line probing (ILP) measures the spontaneous RNA cleavage caused by in-line attack from 2'-hydroxyl to neighboring 3'-phosphate, which lead to RNA phosphodiester backbone scission, and thus 5' and 3' RNA fragments²⁹. In general, the more flexible the RNA nucleotide is, the stronger the in-line cleavage, i.e. band intensity on the gel in this study. We have performed the improved ILP assay on miR-765, 5'-UGGAGGAGAAGGAAGGUGAUG-3' (with a 5'-FAM label, Table S3, ESI†), at single nucleotide resolution (Figure 2) and found an ILP cleavage pattern under K⁺-containing condition that is distinct from Li⁺-containing condition (Figure 2A, lanes 3-4), with a low Pearson's correlation coefficient (PCC) of 0.45. Under K⁺ condition, we observed that the Gs involved in rG4s were more protected from in-line attack compared to the loop sequences (Figure 2A, lane 4). By examining the ratio of K⁺/Li⁺ at every nucleotide, we found that most Gs, except for G12, involved in the rG4 had a ratio of K⁺/Li⁺ <1, indicating those Gs were less flexible in K⁺ (Figure 2B). These results strongly suggested that under physiological K⁺ condition and temperature, rG4 was the predominant structural conformation in miR-765.

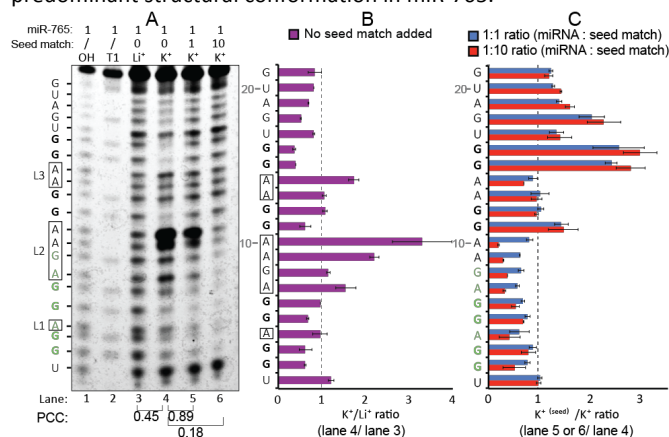


Figure 2. In-line probing (ILP) results and analyses of miR-765. MiR-765, which contains a putative rG4, was subjected to ILP under 150mM Li⁺-containing and 150mM K⁺-containing conditions at physiologically relevant temperature (37°C). **A)** RNA was size-fractionated on denaturing polyacrylamide gel after the ILP reaction. Lane 1 shows the hydrolysis ladder (every nucleotides), lane 2 shows the RNase T1 ladder (Gs only). Lanes 3-6 show ILP cleavage under Li⁺, K⁺, K⁺ plus one equivalent concentration of seed match sequence in mRNA added, and K⁺ plus ten equivalent of seed match sequence in mRNA. The Pearson correlation coefficient (PCC) reports the correlation of band intensities between conditions, with PCC of 1 being perfect positive correlation. **B)** K⁺/Li⁺ ratio report the nucleotides that are more exposed (>1) or protected (<1) by changing from Li⁺ to K⁺ condition. Most nucleotides on the loops of rG4 (L1, L2, L3) are more exposed, whereas most Gs involved in rG4 (bolded Gs) are protected. **C)** K⁺(seed)/K⁺ ratio report the nucleotides that are more exposed (>1) or more protected (<1) by addition of seed match sequence in mRNA (at one or ten equivalent). miRNA

seed region (nucleotides 2-8, green) that interact with the seed match sequence (7 nucleotides, Fig. 1C) are protected. This protection can also be observed visibly on the gel in A. Error bars reported show standard deviations.

We also validated the formation of rG4 in other human miRNAs (miR-149, miR-197, miR-432) that we selected from the bioinformatics analysis (Figures S1-3, Table S3, ESI†). The ILP cleavage pattern and K⁺/Li⁺ ratio of these miRNAs were largely consistent with miR-765 and other reported rG4-containing transcripts³¹, indicating that ILP can report the RNA structural information of miRNA at single nucleotide resolution, and more importantly that rG4s can form in mature miRNAs under physiologically relevant temperature and K⁺ conditions.

To validate the formation of rG4 in miR-765, we attempted to identify the spectroscopic features of rG4s using multiple biophysical assays¹. First, we performed circular dichroism (CD), and found a characteristic positive peak at 262nm under 150 mM K⁺ but not 150 mM Li⁺ condition, consistent with the formation of parallel topology rG4 (Figure 3A). Second, we also conducted fluorescent turn-on assays using G4 ligands such as N-methyl mesoporphyrin IX (NMM) and thioflavin T (ThT), and observed that the fluorescence significantly increased in 150 mM K⁺ versus 150 mM Li⁺ condition (Figure 3B-C), further supporting that the miR-765 folded into rG4 conformation under the physiological K⁺ condition that allowed for G4 ligand recognition and enhanced its fluorescence. Lastly, thermal melting monitored by UV absorbance (UV-melting) were carried out and exhibited the distinct hypochromic shift at 295 nm upon melting, with a melting temperature (T_m) of 45 °C under 150 mM K⁺ condition (Figure 3D), suggesting rG4 in miR-765 is thermostable at physiological K⁺ condition. A slight hysteresis of 3°C was observed (Figure S4, ESI†), which is not uncommon for G4 melting³²⁻³⁴. These biophysical assays were also performed for other miRNA candidates (Figures S5-S7, ESI†), verifying the folding of these miRNAs into rG4 conformations. Concentration-dependent UV melting was performed and the results showed that the T_ms are independent of the oligonucleotide concentration, suggesting intramolecular rG4 folding under our testing conditions (Figure S8, ESI†). In addition, mutants were designed by substituting several Gs to As to preclude rG4 formation in the miRNAs, and the resulting data on mutants all indicated no observable rG4 signatures (Figures S9-S12, Table S3, ESI†), further confirming the contrasting formation of rG4 in the wildtype miRNAs.

For a human miRNA to perform its role, its seed region (nucleotide positions 2-8) has to recognize its cognate mRNA target and form intermolecular RNA-RNA base pair interactions²⁰. We hypothesize that the formation of rG4 structure in a miRNA could potentially influence its bindings with its mRNA targets. To test this, we have designed short RNA oligomers (7 nucleotides long) to mimic the native mRNA sequence that interacts with the seed region of the miRNA (Figure 1C), and investigated the intermolecular RNA-RNA interactions (i.e. miRNA-mRNA in our case) under physiological K⁺ condition and temperature using ILP assay.

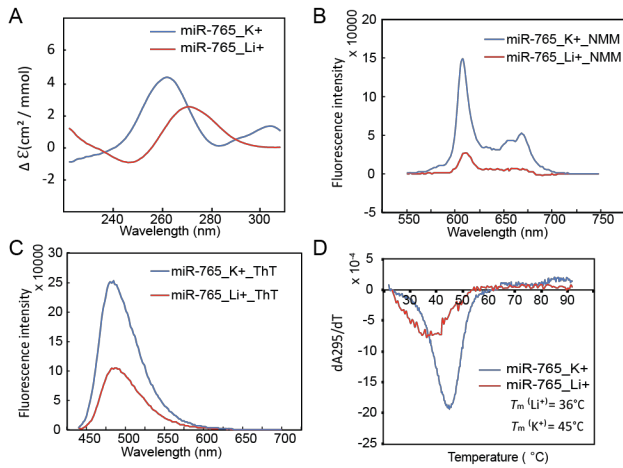


Figure 3. Biophysical characterization of rG4 in miR-765. **A)** CD spectrum shows a distinct signature under K^+ but not in Li^+ conditions, suggesting the formation of a parallel topology rG4. **B-C)** Fluorescence spectra show augmented fluorescence under K^+ as compared to Li^+ conditions, indicating the presence of rG4 for G4 ligands (B. NMM and C. ThT) recognition and fluorescence enhancement. **D)** UV melting shows increased rG4 thermostability from 36°C (Li^+ condition) to 45°C (K^+ condition), suggesting the rG4 is thermostable at physiological temperature under K^+ condition.

Our ILP data revealed three important findings (Figure 2A,C). First, ILP cleavage profile were different between 1:0 ratio of miRNA to seed match sequence in mRNA (no seed match added as control), 1:1 ratio of miRNA to seed match, and 1:10 ratio of miRNA to seed match, as shown by a decrease in PCC from 1 (1:0 ratio) to 0.89 (1:1 ratio) and to 0.18 (1:10 ratio) (Figure 2A), suggesting that the major RNA structural conformation of miR765 (i.e. rG4 in this case under K^+ condition) changes upon seed match addition. This finding is further supported by the results of our UV melting that was performed with and without seed match (Figure S4A-B, ESI†).

Second, we inspected each nucleotide of the miRNA and found that the regions that were strongly protected upon seed match addition coincide with the miRNA regions that are being targeted (nucleotides 2-8) (Figure 2A,C), supporting the formation of intermolecular RNA-RNA base pairing. In addition, we observed that for other region of the miRNA (e.g. nucleotides 11-21), especially those Gs that are involved in rG4 formation (nucleotides 11-12 and 15-16), were more susceptible to in-line cleavages (Figure 2A,C), indicating the unfolding of rG4 upon seed match addition and miRNA-mRNA interaction (nucleotides 2-8), likely causing the other regions of the miRNA (nucleotides 11-21) to be unstructured.

Third, among other miRNA candidates (Figures S1-S3, ESI†), we found that for miR-149 and miR-197, exhibited almost no change upon seed match sequence addition, as indicated by the PCC of 0.99 (1:1) and 0.99 (1:10) for miR-149 (Figure S1, ESI†), and PCC of 0.98 (1:1) and 0.89 (1:10) for miR-197 (Figure S2, ESI†), respectively. In contrast, we found that for miR-432, a small change with a PCC of 0.93 (1:1) and 0.68 (1:10) is detected, and the protection on miRNA was observable visibly on the gel (Figure S3, ESI†). As RNA-RNA base pairing depends on the availability of the RNA bases, we speculate that the more thermostable G-quadruplexes will hinder hybridization of their RNA 7-mer complements, and indeed from our UV melting data, the T_m of miR-149 and miR-197 were higher than that of miR-765 and miR-432 (Figures 3D and S5-7, ESI†), supporting this hypothesis.

Collectively, these structural analyses provide strong evidence for the formation of rG4 in miRNAs under K^+ conditions, and the

addition of seed match sequence in mRNA can influence the rG4 folding for miR-765 and miR-432, but not miR-149 and miR-197, which can be rationalized by the difference in T_m of rG4s of the respective miRNAs determined *in vitro* using UV melting. Importantly, the application of ILP to interrogate miRNA structure and intermolecular RNA-RNA binding is new and offers RNA structural information on miRNAs at single nucleotide resolution.

To investigate the role of rG4 structure in miRNAs and its relationship with miRNA-mediated post-transcriptional regulation, we have generated a reporter plasmid that contains the corresponding wildtype miRNA targeting site in the 3'UTR of the Renilla luciferase mRNA, and performed dual luciferase reporter gene assays on wildtype miRNA mimics (containing the rG4) and scrambled miRNA mimic (as negative control) in HEK-293T cells (Figure 4A). Our results on miR-765 showed that compared to the scrambled miRNA mimic control, ectopic expression of wildtype miR-765 mimic decreased the normalized luciferase activity of the reporter with miR-765 3'UTR by 89% (after normalizing the difference in transfection efficiency using the firefly luciferase), or a 9.1 fold in reduction in the normalized luciferase activity (Figure 4B). To exacerbate the effect of rG4 structure, the transfected cells were treated with a G4 ligand NMM that was previously reported to stabilize rG4 in cells³⁵. UV melting results showed that NMM can stabilize rG4 in miR-765 *in vitro* (Figure S4A,C, ESI†). In cells, we observed that the normalized luciferase activity was rescued from 0.11 ± 0.03 to 0.62 ± 0.02 , or a 5.6 fold rescue effect (Figure 4B).

To ensure that the effect was due to a specific stabilization of rG4 in miRNA by NMM, rather than any general, non-specific NMM effect on the cells, we have also generated a reporter gene plasmid that contains corresponding mutated miRNA targeting site at 3'UTR region of the Renilla luciferase mRNA, and performed dual luciferase reporter gene assays on mutant miRNA mimics (no rG4) and scrambled miRNA mimics (as negative control) in HEK-293T cells (Figure 4A). While the mutant miR-765 mimic inhibited the normalized luciferase activity, treatment with NMM showed no significant rescue effect (Figure 4B), suggesting that the NMM effect observed for the wildtype miR-765 is rG4-specific.

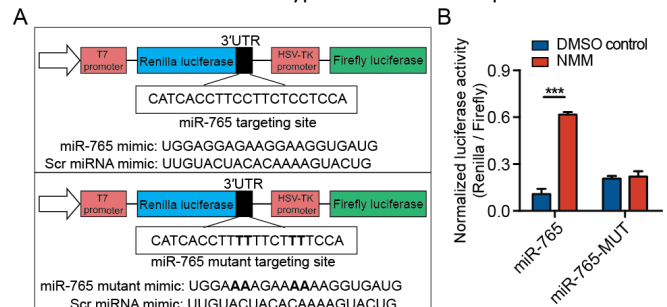


Figure 4. In cell dual luciferase reporter gene assay results and analyses of miR-765. **A)** Schematic of the wildtype and mutant reporter plasmids. The wildtype or mutant miR-765 targeting site was appended to the 3'UTR of Renilla luciferase, whereas the Firefly luciferase is used as control for transfection efficiency. The wildtype or mutant reporters were co-transfected with wildtype or mutant miR-765 mimics, or with scrambled (scr) miRNA mimics as a negative control. **B)** Renilla luciferase activity was normalized to Firefly luciferase activity. Average normalized luciferase activity of the wildtype or mutant reporters 2 days after a co-transfection with wildtype or mutant miR-765 mimics relative to that with the scrambled miRNA mimics. The cells were treated with 80 μ M NMM or DMSO for 2 days after the transfection. Both miR-765 (with rG4 sequence) and miR-765 mutant (rG4 mutant) can suppress luciferase activity of their corresponding reporters, but upon NMM G4 ligand treatment, only the luciferase activity in miR-765 can be rescued, suggesting that rG4 formation and stabilization in miR-765 can alter the luciferase reporter gene product. Normalized

luciferase activity was presented as means \pm SEM of 3 transfection replicates. Statistical significance was analyzed using Student's two-tail t-test. *** $p < 0.001$, relative to DMSO controls.

Similar results were observed for miR-432; however, no effect of NMM was observed for miR-149 and miR-197 cases (Figure S13, ESI†). This finding is largely consistent with the ILP results on miRNA-mRNA interactions (Figures 2 and S1-3, ESI†). Although we cannot rule out the possibility of other contributing factors in cells, it is likely that the highly thermostable rG4s in miR-149 and miR-197 (with higher T_m than miR-765 and miR-432) are predominately folded, thus no NMM effect was observed in cells. This is somewhat supported by the difference in suppression effect of the normalized luciferase activities for miR-149 and miR-197 cases (0.62 ± 0.12 and 0.87 ± 0.17 , respectively), as compared to the normalized luciferase activities for miR-765 and miR-432 (0.11 ± 0.03 and 0.06 ± 0.01 , respectively) (Figures 4 and S12, ESI†). Overall, these reporter gene results demonstrate for the first time that rG4 formation and stabilization in miRNAs can influence gene products in cells.

Our bioinformatics analyses using different G4 prediction tools suitable for RNA identified 166 overlapping, putative rG4s in human miRNAs (6 %), and also in other species (Table S1, ESI†), suggesting that it may be a widespread phenomenon and acts as an additional layer of post-transcriptional regulation at the RNA level. Together with the recently published examples of rG4s in pri-miRNAs and pre-miRNAs, our findings in this work regarding the formation and function of rG4 in miRNAs support the potential roles of rG4 structures in non-coding RNAs, in particular regarding miRNA biogenesis and miRNA-mediated post-transcriptional regulation. Although the cellular factors and status that regulate rG4 folding/unfolding remains largely unknown, we have provided insights in this study that small G4 chemical ligand may be used for the manipulation of rG4 stabilization and folding, and alteration of the gene expression (Figure 4).

In summary, our structural analyses using improved ILP and biophysical assays have demonstrated the formation of rG4 structures in biologically important miRNAs and reported the effect of rG4 formation on miRNA-mRNA interactions at single nucleotide resolution. Using a luciferase reporter gene cellular assay, we have illustrated that rG4 formation and stabilization by G4 ligand addition, e.g. in miR-765, can alter gene expression in cells. Our method and findings offer insights into the structural and biological roles of rG4s in miRNAs, and expand the diversity and complexity of the miRNA-mediated post-transcriptional regulation.

Acknowledgements

This Kwok laboratory is supported by Hong Kong RGC Project No. CityU 21302317, N_CityU110/17, Croucher Foundation Project No. 9500030, and City University of Hong Kong Projects No. 9610363, 7200520. The Le laboratory is supported by the Hong Kong Health and Medical Research Fund (9211101), the Hong Kong Research Grants Council (21106616), and the Natural Science Foundation of China (81602514 and 81773246). The Sahakyan laboratory is supported by MRC Strategic Alliance Funding (MC_UU_12025) to MRC WIMM. We thank Dingpeng Zhang for the discussion.

Conflicts of interest

There are no conflicts to declare

Notes and references

1. C. K. Kwok and C. J. Merrick, *Trends Biotechnol.*, 2017, **35**, 997-1013.
2. C. K. Kwok, G. Marsico and S. Balasubramanian, *Cold Spring Harb Perspect Biol.*, 2018, doi:10.1101/cshperspect.a032284.
3. R. Simone, P. Fratta, S. Neidle, G. N. Parkinson and A. M. Isaacs, *FEBS Lett.*, 2015, **589**, 1653-1668.
4. A. Cammas and S. Millevoi, *Nucleic Acids Res.*, 2017, **45**, 1584-1595.
5. C. K. Kwok, G. Marsico, A. B. Sahakyan, V. S. Chambers and S. Balasubramanian, *Nat. Methods*, 2016, **13**, 841-844.
6. J. U. Guo and D. P. Bartel, *Science*, 2016, **353**, aaf5371.
7. G. Biffi, M. Di Antonio, D. Tannahill and S. Balasubramanian, *Nat. Chem.*, 2014, **6**, 75-80.
8. X. C. Chen, S. B. Chen, J. Dai, J. H. Yuan, T. M. Ou, Z. S. Huang and J. H. Tan, *Angew. Chem. Int. Ed.*, 2018, **57**, 4702-4706.
9. S. Millevoi, H. Moine and S. Vagner, *WIREs RNA*, 2012, **3**, 495-507.
10. S. Kumari, A. Bugaut, J. L. Huppert and S. Balasubramanian, *Nat. Chem. Biol.*, 2007, **3**, 218-221.
11. R. Shahid, A. Bugaut and S. Balasubramanian, *Biochemistry*, 2010, **49**, 8300-8306.
12. A. Arora and B. Suess, *RNA Biol.*, 2011, **8**, 802-805.
13. E. Crenshaw, B. P. Leung, C. K. Kwok, M. Sharoni, K. Olson, N. P. Sebastian, S. Ansaloni, R. Schweitzer-Stenner, M. R. Akins, P. C. Bevilacqua and A. J. Saunders, *PLoS One*, 2015, **10**, e0143160.
14. S. Lattmann, M. B. Stadler, J. P. Vaughn, S. A. Akman and Y. Nagamine, *Nucleic Acids Res.*, 2011, **39**, 9390-9404.
15. H. Martadinata and A. T. Phan, *Biochemistry*, 2013, **52**, 2176-2183.
16. K. Matsumura, Y. Kawasaki, M. Miyamoto, Y. Kamoshida, J. Nakamura, L. Negishi, S. Suda and T. Akiyama, *Oncogene*, 2017, **36**, 1191-1199.
17. S. G. Rouleau, J. M. Garant, F. Bolduc, M. Bisailon and J. P. Perreault, *RNA Biol.*, 2018, **15**, 198-206.
18. C. K. Kwok, A. B. Sahakyan and S. Balasubramanian, *Angew. Chem. Int. Ed.*, 2016, **55**, 8958-8961.
19. G. Mirihana Arachchilage, A. C. Dassanayake and S. Basu, *Chem Biol*, 2015, **22**, 262-272.
20. D. P. Bartel, *Cell*, 2018, **173**, 20-51.
21. W. Tan, J. Zhou, J. Gu, M. Xu, X. Xu and G. Yuan, *Talanta*, 2016, **154**, 560-566.
22. W. Tan, L. Yi, Z. Zhu, L. Zhang, J. Zhou and G. Yuan, *Talanta*, 2018, **179**, 337-343.
23. A. Kozomara and S. Griffiths-Jones, *Nucleic Acids Res.*, 2014, **42**, D68-73.
24. J. M. Garant, J. P. Perreault and M. S. Scott, *Bioinformatics*, 2017, **33**, 3532-3537.
25. J. L. Huppert and S. Balasubramanian, *Nucleic Acids Res.*, 2005, **33**, 2908-2916.
26. Y. K. Leung, Q. K. Y. Chan, C. F. Ng, F. M. T. Ma, H. M. Tse, K. F. To, J. Maranchie, S. M. Ho and K. M. Lau, *Plos One*, 2014, **9**.
27. W. Liang, X. Wei, Q. Li, N. Dai, C. Y. Li, Y. Deng, X. Jiang, X. R. Tan, X. Y. Dai, M. X. Li, C. X. Xu, D. Wang and Z. Y. Zhong, *Journal of Cancer*, 2017, **8**, 1542-1551.
28. B. H. Xie, X. He, R. X. Hua, B. Zhang, G. S. Tan, S. Q. Xiong, L. S. Liu, W. Chen, J. Y. Yang, X. N. Wang and H. P. Li, *Cancer Biomark*, 2016, **16**, 405-413.
29. J. D. Beaudoin, R. Jodoin and J. P. Perreault, *Methods*, 2013, **64**, 79-87.
30. B. Strauss, A. Nierth, M. Singer and A. Jaschke, *Nucleic Acids Res.*, 2012, **40**, 861-870.
31. C. K. Kwok, Y. Ding, S. Shahid, S. M. Assmann and P. C. Bevilacqua, *Biochem J*, 2015, **467**, 91-102.
32. B. Kankia, D. Gvarjaladze, A. Rabe, L. Lomidze, N. Metreveli and K. Musier-Forsyth, *Biophys. J.*, 2016, **110**, 2169-2175.
33. E. Hatzakis, K. Okamoto and D. Yang, *Biochemistry*, 2010, **49**, 9152-9160.
34. J. L. Mergny, A. T. Phan and L. Lacroix, *FEBS Lett.*, 1998, **435**, 74-78.
35. E. O'Day, M. T. Le, S. Imai, S. M. Tan, R. Kirchner, H. Arthanari, O. Hofmann, G. Wagner and J. Lieberman, *J. Biol. Chem.*, 2015, **290**, 17909-17922.